Molecular Crystals and Liquid Crystals
Publication details, including instructions for authors and subscription information:
http://www.tandfonline.com/loi/gmcl16

Molecular Structure, Conformation and Orientational Order of Para-Azoxy-Anisole (PAA) in the Nematic Phase, and Their Temperature Dependence: Results from a Deuterium and Proton Magnetic Resonance Study

A. J. Dianoux [a] , J. B. Ferreira [b] , A. F. Martins [b] , A. M. Giroud [c] & F. Volino [c]

[a] Institut Laue-Langevin, 156X, 38042, Grenoble, Cédex, France

[b] Centro de Fisica da Materia Condensada, INIC, 2 Av. Gama Pinto, 1699, Lisboa, Codex, Portugal

[c] Département de Recherche Fondamentale, Centre Etudes Nucléaires de Grenoble, 85X, 38041, Grenoble, Cédex, France

Version of record first published: 20 Apr 2011.

Mol. Cryst. Liq. Cryst., 1985, Vol. 116, pp. 319–352
0026-8941/85/1164–0319/$30.00/0

Molecular Structure, Conformation and Orientational Order of Para-Azoxy-Anisole (PAA) in the Nematic Phase, and Their Temperature Dependence: Results from a Deuterium and Proton Magnetic Resonance Study†

A. J. DIANOUX

Institut Laue-Langevin, 156X, 38042 Grenoble Cédex, France

J. B. FERREIRA and A. F. MARTINS

Centro de Fisica da Materia Condensada, INIC, 2 Av. Gama Pinto, 1699 Lisboa Codex, Portugal

A. M. GIROUD‡ and F. VOLINO§¶

Département de Recherche Fondamentale, Centre d'Etudes Nucléaires de Grenoble, 85X, 38041 Grenoble Cédex, France

(*Received June 15, 1983; in final form August 17, 1984*)

Deuterium and proton magnetic resonance data of fully deuterated, partially deuterated on the rings and on the methyl groups, and fully protonated nematic para-azoxyanisole (PAA) are analysed self-consistently in terms of molecular structure, conformation and orientational order using a single order parameter model. The values and

†A preliminary account of this work was presented at the 9th International Conference on Liquid Crystals, Bangalore, India, 6–10 December 1982.

‡Member of CNRS, LA 321.

§Member of CNRS, Equipe de Physico-Chimie Moléculaire, Service de Physique.

¶To whom correspondence should be addressed.

temperature dependences of the nematic order parameter and of some conformational averages are deduced. These results are discussed in the light of results obtained by other methods: X-ray diffraction, quantum chemistry calculations, macroscopic measurements. The influence of partial deuteration, density and temperature on molecular properties is discussed in detail. A simple picture for the nematic phase is proposed. A method and simple relations are given to analyse NMR data of PAA dissolved in fluid anisotropic media.

1. INTRODUCTION

Nuclear Magnetic Resonance (NMR) is presently one of the most accurate methods to obtain information concerning the molecular structure, conformation and orientational order in liquid crystalline media. However, geometrical and dynamical aspects are intimately mixed and it is generally difficult to extract the separate information from the data.

In previous papers [1, 2, 3] we developed a model to interpret quantitatively the relative temperature dependences of deuterium magnetic resonance (DMR) splittings in the (fluid) smectic C, smectic A and nematic phases of terephtal-bis-butyl-aniline (TBBA) [1, 3] and in the nematic phase of para-azoxy-anisole (PAA) [2]. In this model, the molecular motions are split into external and internal motions, which are assumed to be uncoupled. The external motions are pictured as uniform rotation around the long molecular axis, and fluctuations of this axis about the director. The internal motions are described as hindered rotations of molecular fragments around single covalent bonds. An essential feature of this model is to assume that some internal averages depend on temperature mainly as a consequence of the variation of the molecular free volume [2].

In the particular case of PAA, which has extensively been studied by DMR [4–8], the most recent study [5] convincingly shows that the assignment of some DMR lines used in [2], but also in previous works [7, 8], is incorrect. In addition, at variance with what is found for the anisole molecule dissolved in nematic solvents, [9, 10], and assumed in [2], the average conformation of the anisole moieties in nematic PAA is probably not planar [4].

In addition to these results, analysis of DMR and PMR data from methyl deuterated PAA (PAAd6) and ring deuterated PAA (PAAd8), using a method similar to that used for small molecules in a nematic solvent, led the authors of [4] to a very unexpected conclusion: namely that selective deuteration induces important changes in the molecular geometry and/or alignment of PAA in the nematic state.

In this paper, we reexamine most of the DMR and PMR data concerning PAAd14, PAAd8, PAAd6 and normal PAA, in terms of the model used in [2], taking into account the results of [4, 5] concerning the assignment of lines and the conformation of the anisole moieties. The aim is double: first to test more severely the model of [2], and second to check the conclusions of [4] concerning the influence of selective deuteration. We find that the model can explain self-consistently the whole set of data, with results which are basically the same as those of [2] without the need of invoking significant changes due to deuteration.

In section 2, we describe the experimental NMR results for all samples. The theoretical expressions for the splittings and some details on the model are given in section 3. In section 4, we analyse the data and give the results obtained concerning order parameter, structural angles and conformational averages. In section 5, we discuss these results in detail: we give useful relations between splittings and order parameter; we deduce the ortho-interproton distances, estimate conformational angles and discuss the nature of the internal motions. In section 6, these results are compared with relevant results obtained by other methods and a simple picture for the nematic phase is proposed. In the Appendix, we analyse the dipolar splittings between ring deuterons and methyl protons of PAAd8.

2. EXPERIMENTAL RESULTS

NMR spectra were obtained using two pulsed NMR Brüker spectrometers: a WM 250 spectrometer working at 38.4 MHz for DMR and a CXP 100 spectrometer, working at 75 MHz for PMR. Temperature homogeneity in the samples was estimated to be ~0.5°C. Spectra were taken in the whole nematic range by slowly cooling from the isotropic phase, by steps of 1 to 3 degrees. Clearing point temperatures T_K as measured in the NMR experiments are: 407.5 ± 0.5 K for PAAd14, 408 ± 0.5 K for PAAd8, 409 ± 0.5 K for PAAd6 and 409 ± 0.5 K for PAA.

Figure 1 shows a typical DMR spectrum of PAAd14. It is similar to the published ones [5–7]. The correct [4, 5] assignment of splittings is indicated, namely $\Delta\nu_1$, $\Delta\nu_4$, $\Delta\nu_6$, correspond to one anisole moiety (say A), and $\Delta\nu_2$, $\Delta\nu_5$, $\Delta\nu_3$ correspond to B. This notation for splittings is the same as used in previous works [7, 2]. The lines corresponding to deuterons (3′,5′) and (3,5) are split by dipole-dipole interactions with deuterons (2′,6′) and (2,6) respectively. This defines two dipolar splittings $\Delta\nu_{dip}^{A,DD}$ and $\Delta\nu_{dip}^{B,DD}$ as indicated.

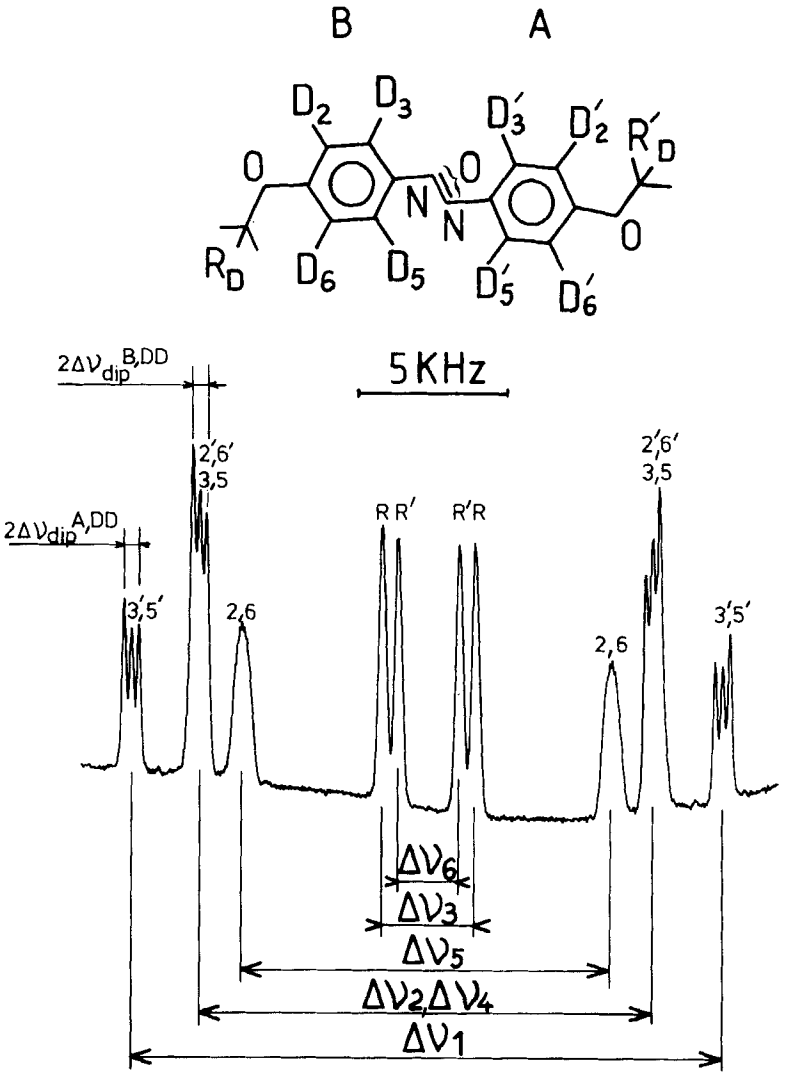

FIGURE 1 38.4 MHz DMR spectrum of PAAd14 in the supercooled nematic phase. The assignment of lines is that of references [4, 5] but the location of the oxygen atom of the azoxy moiety cannot be specified. The definition of the splittings is the same as in references [2, 7], with the convention that $\Delta\nu_4$ corresponds to the broad line underlying the sharp triplet corresponding to $\Delta\nu_2$.

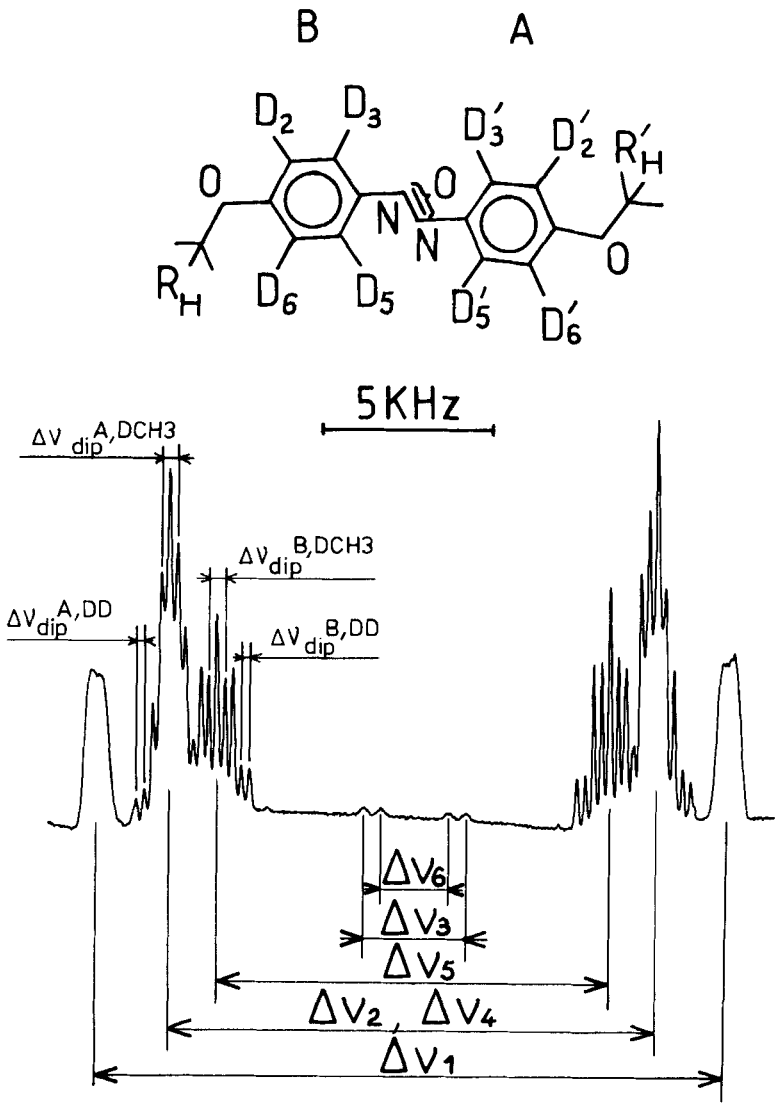

FIGURE 2 Idem as Figure 1 for PAAd8.

Figure 2 shows a similar spectrum for PAAd8. The sample contained a few percent of completely deuterated molecules as can be inferred from the two small methyl deuteron doublets $\Delta\nu_3$ and $\Delta\nu_6$. This allows the measurement of the six DMR splittings as for PAAd14. The lines corresponding to deuterons (2',6') and (2,6) are split by

both dipole-dipole interaction with deuterons (3′,5′) and (3,5) and by dipole-dipole interaction with methyl protons R'_H and R_H [4]. This defines four dipolar splittings, $\Delta\nu_{dip}^{A,DD}$ and $\Delta\nu_{dip}^{B,DD}$ as with PAAd14, and $\Delta\nu_{dip}^{A,DCH_3}$ and $\Delta\nu_{dip}^{B,DCH_3}$, as indicated (see the Appendix).

Figure 3 shows the DMR spectrum of PAAd6. The central part corresponds to the methyl deuterons which are split by dipolar interaction with the neighbouring phenyl protons [4]. The four small lines in the outer part of the spectrum correspond to phenyl deuterons. High resolution PMR of this molecule in solution shows that

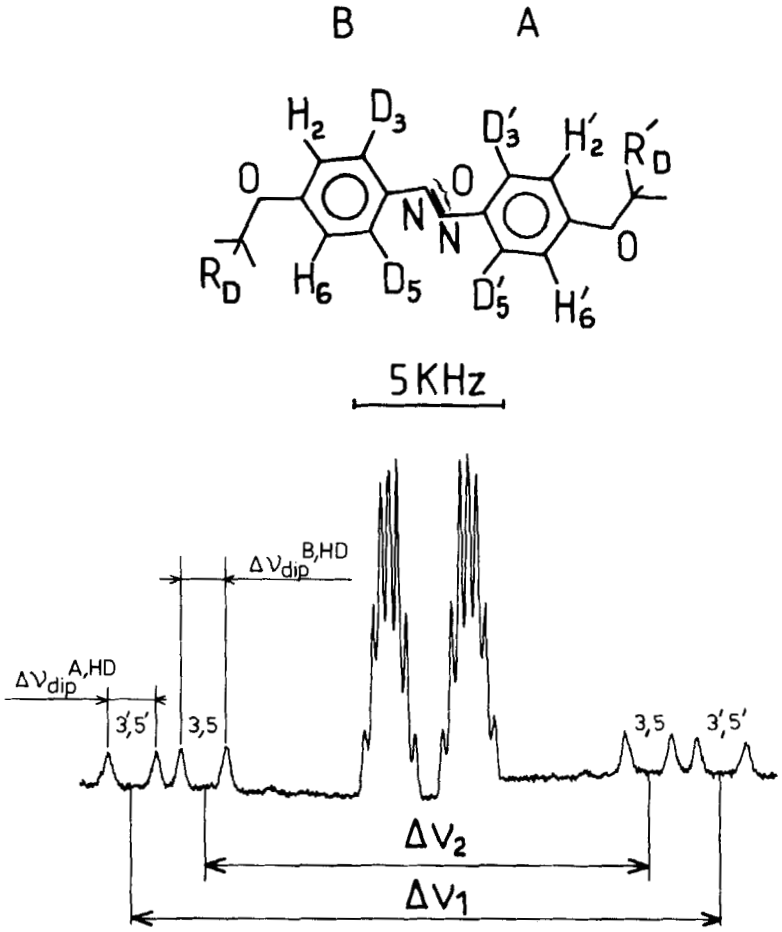

FIGURE 3 Idem as Figure 1 for PAAd6. Only ~10% of the molecules are deuterated on the rings as indicated.

these lines should be assigned to deuterons in positions (3′,5′) and (3,5) which are split by protons in positions (2′,6′) and (2,6) respectively. This means that during the synthesis of this molecule, not only the methyl groups, but also ~10% of the rings in the above mentioned positions were deuterated. This permits the measurement of the two quadrupolar splittings $\Delta\nu_1$ and $\Delta\nu_2$, and of the dipolar splittings $\Delta\nu_{dip}^{A,HD}$ and $\Delta\nu_{dip}^{B,HD}$, as indicated.

Figure 4 shows typical PMR spectra of PAA (a) and PAAd6 (b) at the same reduced temperature. Both exhibit a large doublet Δ' and Δ, mainly due to dipolar interaction between orthoprotons, whose lines show up some structure. In addition, PAA contains a central feature to be attributed to the methyl protons. Such spectra are similar to those published elsewhere (e.g. [11]).

3. THEORETICAL EXPRESSION OF QUADRUPOLAR AND DIPOLAR SPLITTINGS

The theoretical expressions for the splittings have been derived in [2] in the hypothesis where the internal rotations of the phenyl and methoxy groups have C_{2v} symmetry, assuming a planar most probable conformation for the anisole moieties. Release of this last condition only slightly changes the expressions of the methyl deuterons quadrupolar splittings by introducing a quantity T_{AM} as indicated below. The quadrupolar splittings associated with anisole moiety A are [2]:

$$\Delta\nu_{r_1}^{A} = \frac{3}{2} c_{r_1}^{A} \cdot S \cdot \left[P_2(\cos u_{r_1}^{A}) P_2(\cos \epsilon_A) + \frac{3}{4} \sin^2 u_{r_1}^{A} \sin^2 \epsilon_A \cdot T_A \right] \quad (1A)$$

$$\Delta\nu_{r_2}^{A} = \frac{3}{2} c_{r_2}^{A} \cdot S \cdot \left[P_2(\cos u_{r_2}^{A}) P_2(\cos \epsilon_A) + \frac{3}{4} \sin^2 u_{r_2}^{A} \sin^2 \epsilon_A \cdot T_A \right] \quad (2A)$$

$$\Delta\nu_{m}^{A} = -\frac{1}{2} c_{m}^{A} \cdot S \cdot \left[P_2(\cos u_{m}^{A}) P_2(\cos \epsilon_A) + \frac{3}{4} \sin^2 u_{m}^{A} \sin^2 \epsilon_A \cdot T_{AM} \right] \quad (3A)$$

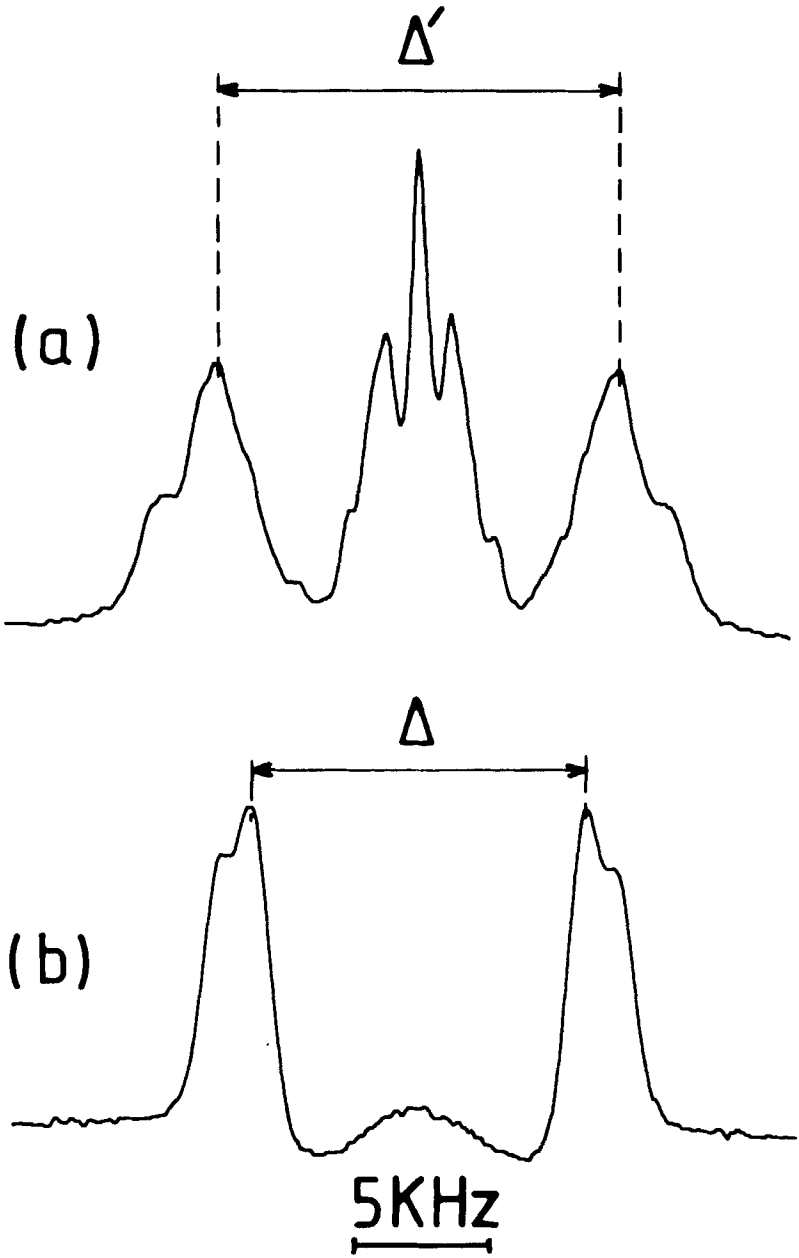

FIGURE 4 75 MHz PMR spectra of normal PAA(a) and PAAd6(b) at the same reduced temperature $T^* = 0.955$, recorded in the same experimental conditions. Note the differences in shapes and peak positions.

with

$$T_A = \langle \cos 2\psi'_A \rangle \cos 2\phi_A \tag{4A}$$

$$T_{AM} = \langle \cos 2\psi'_{AM} \rangle \cos 2\phi_{AM} \tag{5A}$$

The dipolar splittings between spins in ortho-positions on the rings are:

$$\Delta\nu_{dip}^{A,DD} = -\frac{h\gamma_D^2}{2\pi^2 r_A^3} P_2(\cos \epsilon_A) \cdot S = -K_{DD}^A \cdot S \tag{6A}$$

$$\Delta\nu_{dip}^{A,HD} = -K_{HD}^A \cdot S = -\frac{\gamma_H}{\gamma_D} K_{DD}^A \cdot S \tag{7A}$$

Similar equations labeled (1B) to (7B) can be written for moiety B. In these expressions, the c_i are quadrupolar coupling constants: we shall use $c_{r_1} = c_{r_2} = 185$ KHz and $c_m = 172$ KHz as in [2]. The u_i are the angles of the various CD_i bonds for the rings, and of the O-Methyl bond for the methoxy group, with the corresponding internal rotation axes Oz_A and Oz_B, associated with each anisole moiety. The sets (ϵ_A, ϕ_A) and (ϵ_A, ϕ_{AM}) are polar and azimuthal angles of the long molecular axis Oz_o in frames attached to the most probable ring A and to the most probably methoxy group A. These frames are such that the z axis is identical to Oz_A and the x axis is in the symmetry plane of the corresponding group. Similar definitions are used in fragment B. A most probable molecular fragment belongs to a most probable molecular conformation defined as a conformation such as all dihedral angles between fragments correspond to minima of the mean potentials hindering the rotations around these bonds. The quantities ψ'_A and ψ'_{AM} are the current angles describing the rotations around Oz_A of the ring and of the methoxy group, relative to their most probable positions. Consequently $\langle \cos 2\psi'_A \rangle$ and $\langle \cos 2\psi'_{AM} \rangle$ are motional averages which are related to the degree of uniformity of the internal rotations (idem for B).

Most of these notations have been used in [2] and are illustrated in Figure 5 where we show the sketches of a lateral view of one anisole moiety and the view, along the para-axes of the rings (assumed to be parallel), of one possible most probable conformation of the PAA molecule.

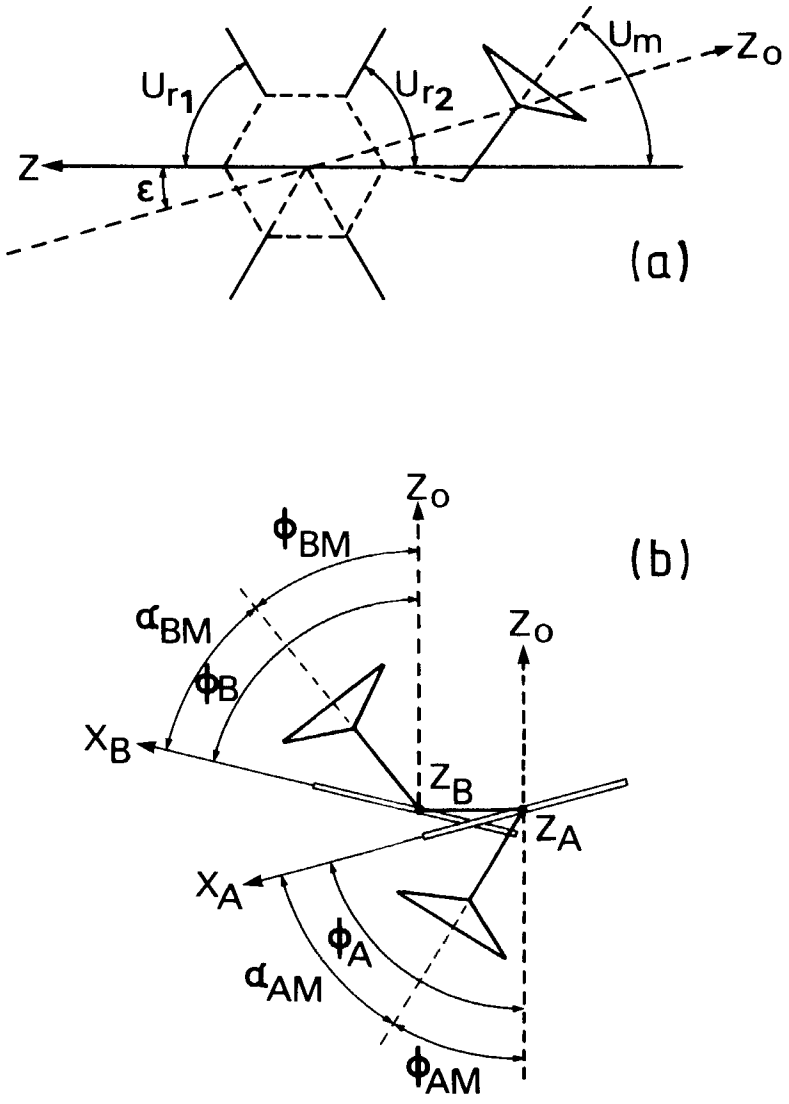

FIGURE 5 Sketch showing the definition of the various axes and angles which are useful in the calculation of the DMR splittings.
a) Lateral view of one anisole moiety in a planar conformation
b) Top view along the para-axis of the rings assumed to be parallel, of the most probable conformation.

4. ANALYSIS OF THE DMR DATA

4a. Quadrupolar splittings

The six quadrupolar splittings $\Delta\nu_i$ (i = 1 to 6) have been measured for about 20 temperatures in the nematic phase, so that $\sim 6 \times 20 = 120$ independent data are available for each experiment. According to Eqs. (1A) to (6B), the problem contains 5 temperature dependent parameters, namely S, T_A, T_B, T_{AM}, T_{BM} and 8 constant angles, namely six u and two ϵ; that is $5 \times 20 + 8 = 108$ parameters. A general fit is possible in these conditions. However, the problem can be considerably reduced by considering both order parameter results and so-called "ratio-plots" [12].

i) combining ^{13}C NMR and optical measurements, and using convincing arguments concerning local field corrections and scaling factors, it has been shown [13] that for PAA, S is very well represented in the whole nematic range, by the following empirical law

$$S = S_o \left(1 - \frac{T}{T^+}\right)^{\gamma} \tag{8}$$

with $S_o = 1.13 \pm 0.03$; $\gamma = 0.189 \pm 0.08$ and $T^+ = T_K + 1.8 \pm 0.3$ K where T_K is the clearing point temperature.

In [2], we showed that the values of S predicted by the model were in good agreement with this relation. Here, in order to reduce the number of parameters, we assume that S is given by Eq. (8) taking for values of S_o, γ and $T^+ - T_K$ the above central values of [13].

ii) the "ratio plot" representation was first [12] introduced as the consequence of the observation that in some liquid crystal phases, if $\Delta\nu_i$, $\Delta\nu_j$, $\Delta\nu_k$ are splittings associated with three inequivalent CD bonds, the plot $\Delta\nu_i/\Delta\nu_k$ versus $\Delta\nu_j/\Delta\nu_k$ is a straight line within experimental accuracy. For PAA, since we have five different quadrupolar splittings ($\Delta\nu_2$ and $\Delta\nu_4$ cannot be discriminated) one can form ten such independent plots. For our model, it is worth considering the two plots formed with the three splittings associated with each anisole moiety. Figures 6 and 7 represent $\Delta\nu_1/\Delta\nu_6$ versus $\Delta\nu_4/\Delta\nu_6$ (associated with A) and $\Delta\nu_2/\Delta\nu_3$ versus $\Delta\nu_5/\Delta\nu_3$ (associated with B) for PAAd8, and it is observed that these curves are indeed very good straight lines. Looking at Eqs. (1A) to (3A) (and 1B to 3B), it is easily seen that, for the model, perfect linearity simply means that T_A is proportional to T_{AM} (and T_B to T_{BM}). We thus have:

$$T_{AM} = \lambda_A \cdot T_A \tag{10A}$$

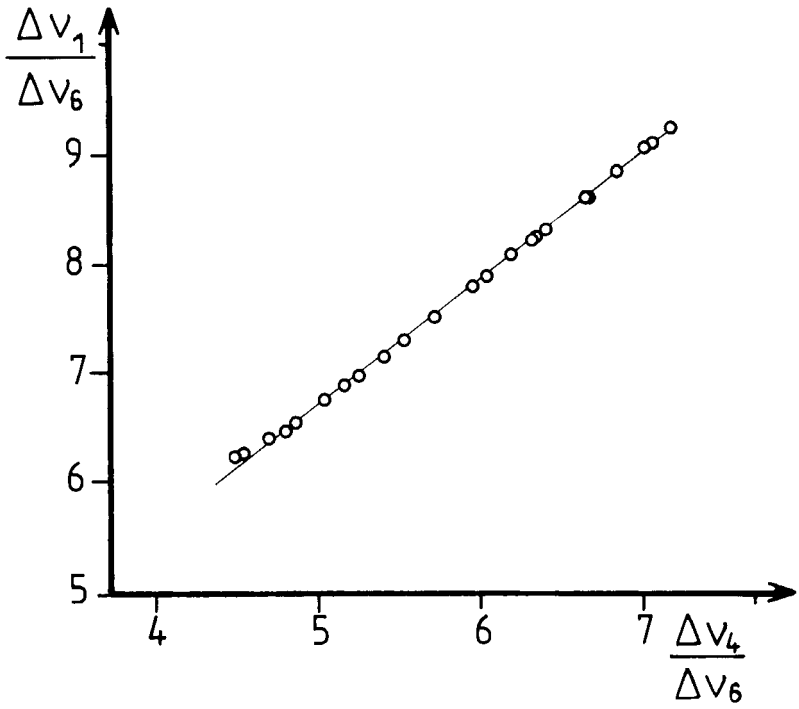

FIGURE 6 "Ratio plot" $\Delta\nu_1/\Delta\nu_6$ versus $\Delta\nu_4/\Delta\nu_6$ associated with anisole moiety A. The full line is the theoretical straight line Eq. (11A) calculated using the values of the parameters found in the fit and the following signs for the splittings: $\Delta\nu_1 = -\Delta\nu^A_{r_1}$, $\Delta\nu_4 = -\Delta\nu^A_{r_2}$, $\Delta\nu_6 = \Delta\nu^A_m$.

and a similar equation for B, where λ_A and λ_B are two new constant parameters.

A straightforward calculation shows that we have for A:

$$\frac{\Delta\nu^A_{r_1}}{\Delta\nu^A_m} = \frac{\sin^2 u^A_{r_1} - \lambda_A \sin^2 u^A_m + \frac{3}{2}(\lambda_A - 1)\sin^2 u^A_{r_1}\sin^2 u^A_m}{\sin^2 u^A_{r_2} - \lambda_A \sin^2 u^A_m + \frac{3}{2}(\lambda_A - 1)\sin^2 u^A_{r_2}\sin^2 u^A_m} \cdot \frac{\Delta\nu^A_{r_2}}{\Delta\nu^A_m} + 3\frac{c^A_r}{c^A_m}\frac{\sin^2 u^A_{r_1} - \sin^2 u^A_{r_2}}{\sin^2 u^A_{r_2} - \lambda_A \sin^2 u^A_m + \frac{3}{2}(\lambda_A - 1)\sin^2 u^A_{r_2}\sin^2 u^A_m} \tag{11A}$$

and a similar equation for B.

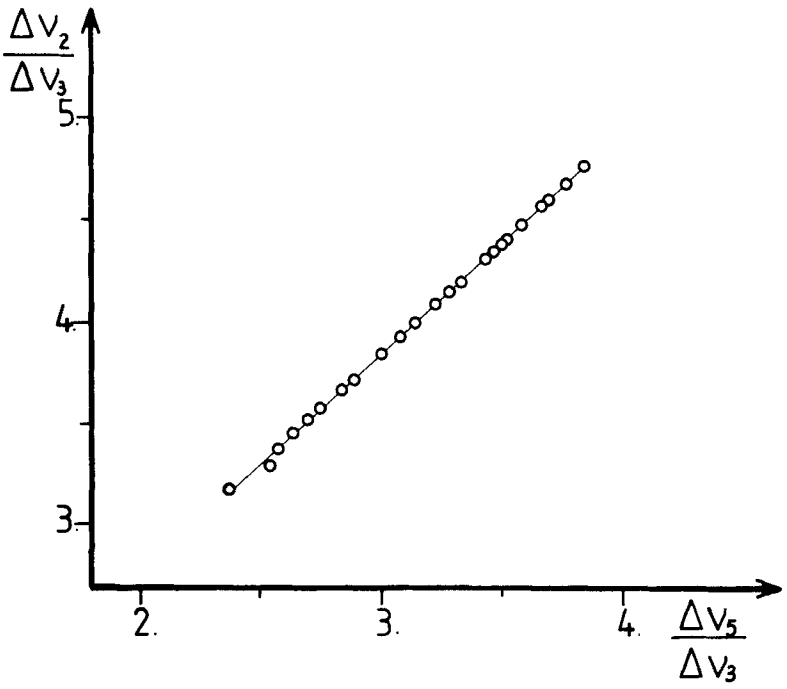

FIGURE 7 Idem as Figure 6 for anisole moiety *B*.

Taking into account (i) and (ii), we are left in the analysis with only two temperature dependent parameters T_A and T_B, and ten constant parameters namely six u, two ϵ and two λ; that is $2 \times 20 + 10 = 50$ parameters to be determined with ~120 data.

This problem was solved in a very similar manner as in [2]. The question of the signs of the splittings was first considered [2]. Obviously, the ring deuteron splittings $\Delta\nu_{r_i}$ are all negative, since the u_r are significantly larger than the "magic angle" 54.74°. The sign of the methyl splittings is less obvious. In [2], we were forced to assume that they are also negative, and it can be shown that this was a consequence of the assumption that the most probable anisole moieties were planar. Since the mean dihedral angles α_{AM} and α_{BM} between the rings and corresponding methoxy groups are probably rather large [4], the sign should be reversed, namely the $\Delta\nu_m$ are probably positive.

With this choice of signs, very good fits were obtained for both PAAd14 and PAAd8 data, for some values of the 50 parameters. In order to test the self-consistency of the analysis concerning S, we

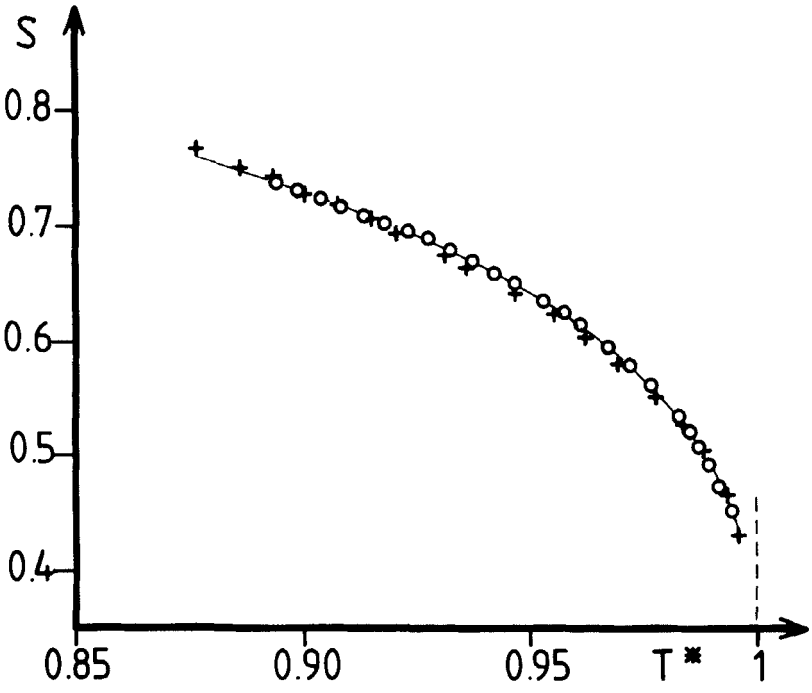

FIGURE 8 Nematic order parameter values obtained for the fit of the model to the quadrupolar splittings, versus reduced temperature: +: from data of PAAd14; 0: from data of PAAd8. The full curve represents Eq. (12).

have fixed the parameters to the found values and tried to change S in order to improve the fit. After several trials, we found that the fit can be only slightly improved. Fitting the new values of S with Eq. (8) taking S_o, γ and T^+ as parameters, yields:

$$S = 1.1237 \left(1 - \frac{T}{T^+}\right)^{0.187} \tag{12}$$

with $T^+ = 409.39 \pm 0.10$ K for PAAd8 and 408.83 ± 0.14 K for PAAd14.

These values found for S_o, γ and T^+ are well inside the error bars showing that the model predicts the same values of the order parameter as optics and ^{13}C NMR [13] within experimental accuracy. Figure 8 shows the best fitted values of S versus reduced temperature $T^* = T/T_K$, ($T_K = T^+ - 1.8$ K) as well as the theoretical curve given by Eq. (12).

We now give the values of the structural and conformational parameters found in the fits, for PAAd8 and PAAd14 (between parenthesis for the latter).

(i) structural angles u:

$$u_{r_1}^A = 57.86° \ (57.88°); \ u_{r_2}^A = 56.91° \ (56.88°); \ u_m^A = 56.80° \ (56.78°)$$

$$u_{r_1}^B = 56.85° \ (56.83°); \ u_{r_2}^B = 56.22° \ (56.23°); \ u_m^B = 57.60° \ (57.58°)$$

(ii) inclinations of the internal rotation axes Oz_A and Oz_B on the long axis Oz_o:

$$\epsilon_A = 15.10° \ (15.10°); \ \epsilon_B = 15.61° \ (15.61°)$$

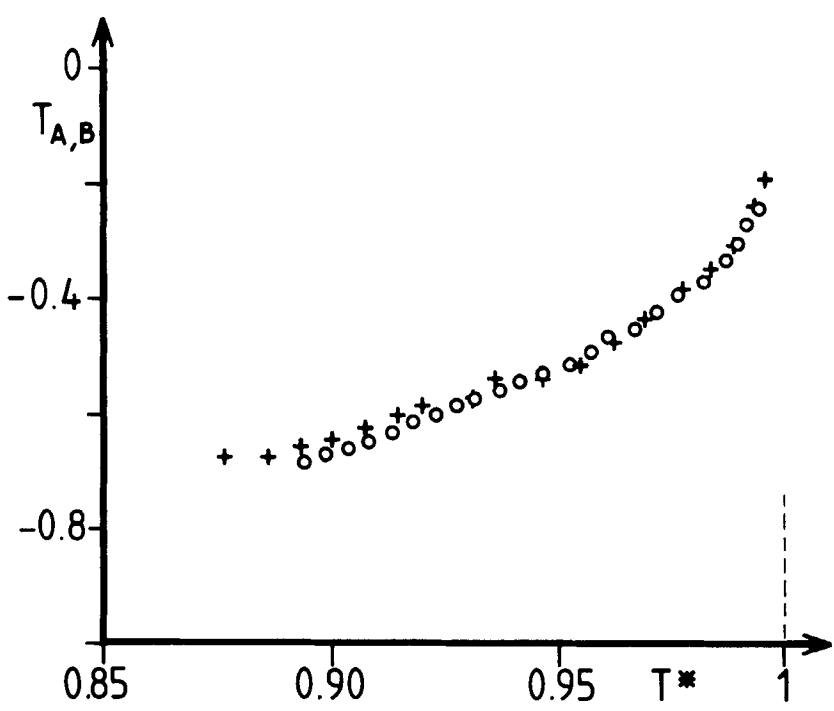

FIGURE 9 Conformational parameters T_A and T_B obtained from the fit of the model to the quadrupolar splittings, versus reduced temperature. In fact T_A and T_B are undiscernable on the figure so that we have put $T_A \simeq T_B \simeq T_{AB}$. +: from data of PAAd14; 0: from data of PAAd8.

(iii) conformational constants λ_A and λ_B:

$$\lambda_A = -0.526\ (-0.526);\ \lambda_B = -0.526\ (-0.526)$$

(iv) the conformational averages T_A and T_B are shown in Figure 9. In fact, for both samples, we found $T_A \approx T_B \approx T_{AB}$ so that only T_{AB} is shown for PAAd8 and PAAd14.

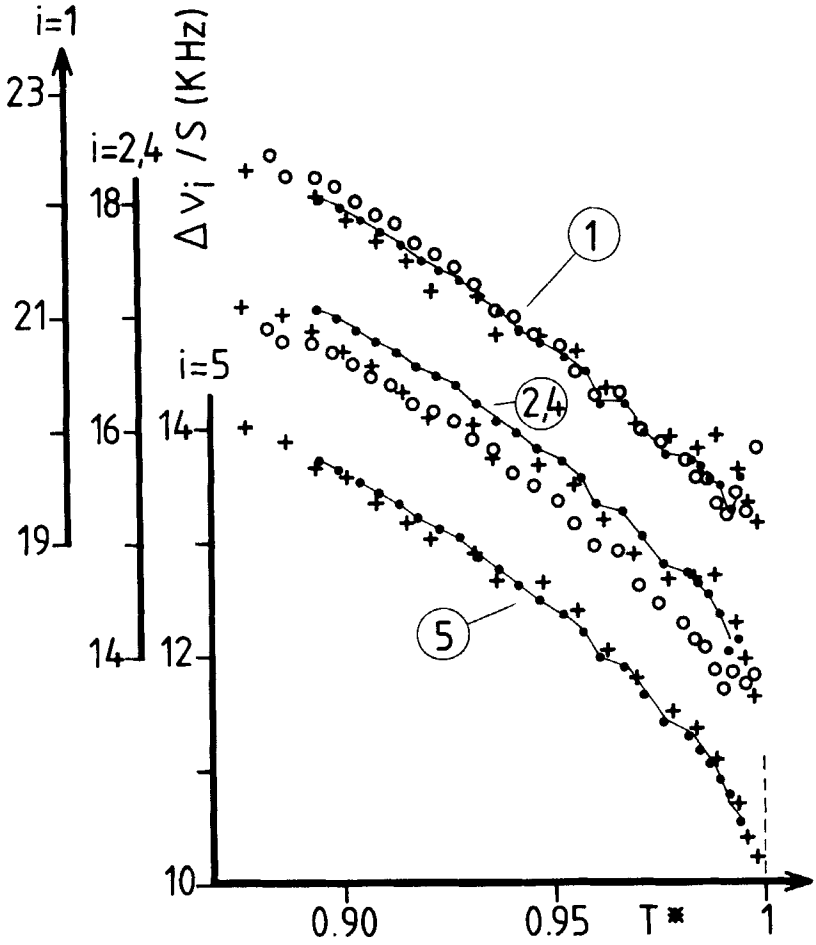

FIGURE 10 Normalized splittings $\Delta\nu_i/S$ versus reduced temperature for i = 1,2,4,5 (phenyl deuterons); $\Delta\nu_i$ are the experimental quadrupolar splittings and S is given by Eq. (12). +: PAAd14; •: PAAd8; 0: PAAd6. The full line corresponds to calculated values for PAAd8.

The overall quality of the fit is characterized by the mean square deviation δ_{fit} between experimental and calculated splittings [2]. This deviation is 16.7 Hz for PAAd8 and 27.6 Hz for PAAd14, both of the order of the experimental uncertainty. It is also pictured in Figures 6 and 7 where the full straight lines are calculated using Eqs. (11A, 11B) taking into account the correct signs of the splittings.

Figures 10 and 11 show all the quadrupolar splittings which could be measured with the three deuterated samples used, versus reduced temperature. Calculated values are also shown for PAAd8. We have chosen to divide the data by S, given by Eq. (12) in order to emphasize the temperature dependence of the conformational quantities T_A, T_B, T_{AM}, T_{BM}. In the present case, the opposite variations for ring and methyl $\Delta\nu_i/S$ come from the different signs of T_A, T_B relative to T_{AM}, T_{BM}, as illustrated by the negative values of λ_A and λ_B found in the fits (Eqs. 10A, B).

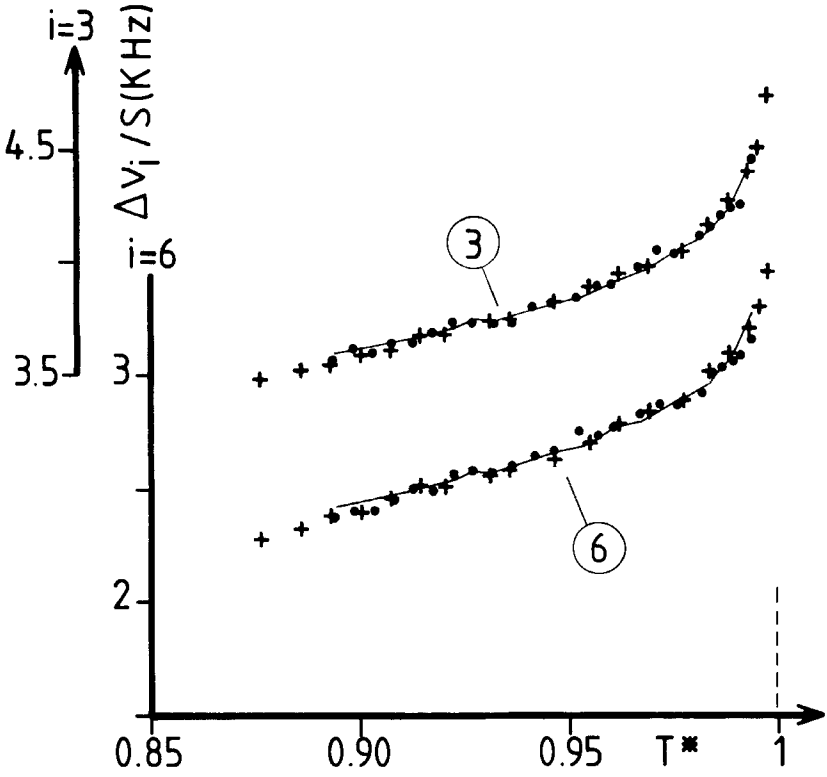

FIGURE 11 Idem as Figure 10 for i = 3,6 (methyl deuterons).

4b. Dipolar splittings

In addition to the quadrupolar splittings, all the dipolar splittings were also measured. $\Delta\nu_{dip}^{A,DD}$ and $\Delta\nu_{dip}^{B,DD}$ could be measured on both PAAd14 and PAAd8 spectra (Figures 1 and 2). Figure 12 shows the results of the measurements using PAAd14 data, and it is seen that, although the experimental precision is relatively poor, we definitely find that $\Delta\nu_{dip}^{A,DD} > \Delta\nu_{dip}^{B,DD}$. The precision is worse with PAAd8 spectra especially for A, but the results for both samples are completely consistent with one another.

$\Delta\nu_{dip}^{A,HD}$ and $\Delta\nu_{dip}^{B,HD}$ were measured on PAAd6 spectra (Figure 3) and are shown in Figure 13. The precision is much better here and the results confirm the nonequality of the two dipolar splittings. Fitting Eqs. (7A, B) to the data, where S is given by Eq. (12), taking K_{HD}^{A}, K_{HD}^{B} and T^{+} as parameters yields $K_{HD}^{A} = 2137 \pm 4$ Hz, $K_{HD}^{B} = 2029 \pm 6$ Hz and $T^{+} = 410.20 \pm 0.10$ K. The full lines in Figure 13 are the theoretical curves calculated using these values. From Eqs. (7A, B) we can deduce K_{DD}^{A} and K_{DD}^{B}. With $\gamma_H/\gamma_D = 6.5123$, we obtain $K_{DD}^{A} = 328$ Hz and $K_{DD}^{B} = 312$ Hz. The full curves in Figure

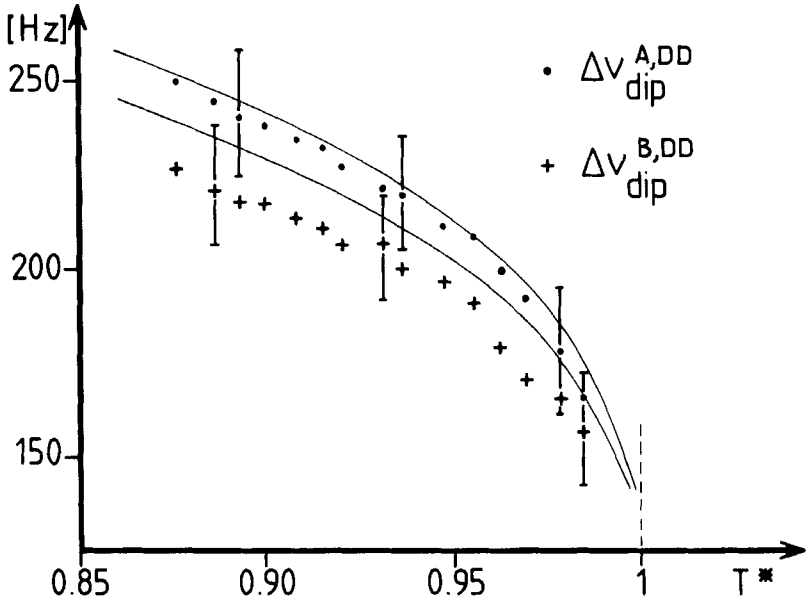

FIGURE 12 Dipolar splittings $\Delta\nu_{dip}^{A,DD}$ and $\Delta\nu_{dip}^{B,DD}$ measured on PAAd14 spectra (Figure 1) versus reduced temperature. The full curves are theoretical as predicted by the model (see section 4b for details).

12 are the theoretical curves calculated using these values in Eqs. (6A, B). Again the temperature dependence is well reproduced and the agreement in absolute values is very good for A, only fair for B. The systematic deviation of ~5% for B is probably due, to a large extent, to the difficulty in pointing accurately three small peaks non-symmetrically superimposed on a broader line (Figure 1).

Dipolar splittings between ring deuterons and methyl protons were deduced from PAAd8 DMR spectra (Figure 2). Figure 14 shows the results versus reduced temperature. Although the A splitting measurements become very imprecise for $T^* > 0.95$, we find, to experimental accuracy

$$\Delta\nu_{dip}^{A,DCH_3} \approx \Delta\nu_{dip}^{B,DCH_3} \tag{13}$$

Concerning the temperature dependence, we have tried to fit to the B data an equation of the form

$$\Delta\nu_{dip}^{B,DCH_3} = K_{DCH_3}^{B} \cdot S \tag{14B}$$

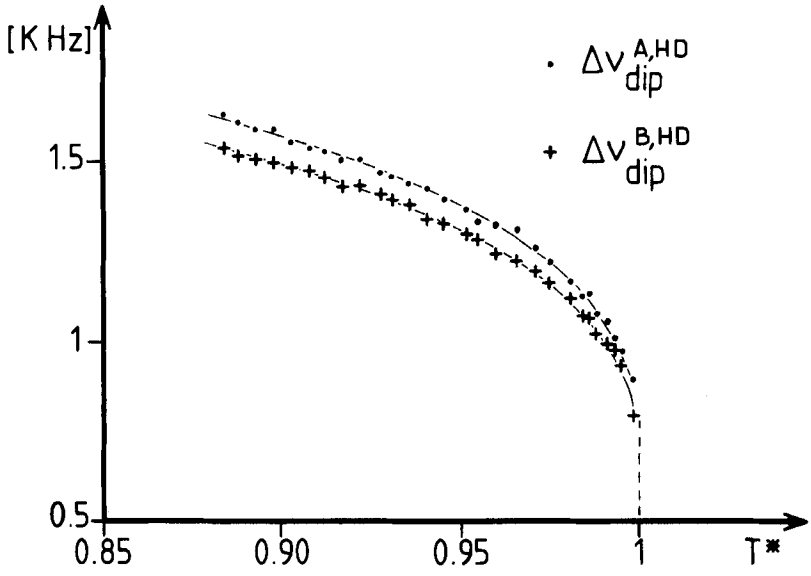

FIGURE 13 Dipolar splittings $\Delta\nu_{dip}^{A,HD}$ and $\Delta\nu_{dip}^{B,HD}$ measured on PAAd6 spectra (Figure 3) versus reduced temperature. The full curves are Eqs. (17) and (18) where S is given by Eq. (12).

where S is given by Eq. (12), taking $K^B_{DCH_3}$ as single parameter. A good fit is found for $K^B_{DCH_3} = 665 \pm 2$ Hz, as can be seen in Figure 14 where the full curve is calculated using this value. This result means that although the conformational averages T_B and T_{BM} vary significantly with temperature (cf. Figure 9), this does not affect the mean dipolar interaction between phenyl deuterons and methyl protons. This result is a consequence of the relative rigidity of the anisole moieties (cf. the Appendix).

For PMR, the detailed calculation of line shapes is rather complicated [11]. However, we have tried the same fit as before to the splittings Δ and Δ' as defined in Figure 4. Figure 15 shows their variation versus reduced temperature and the full curves are the best fits of functions of the form

$$\Delta = K_{HH} \cdot S; \qquad \Delta' = K'_{HH} \cdot S \tag{15}$$

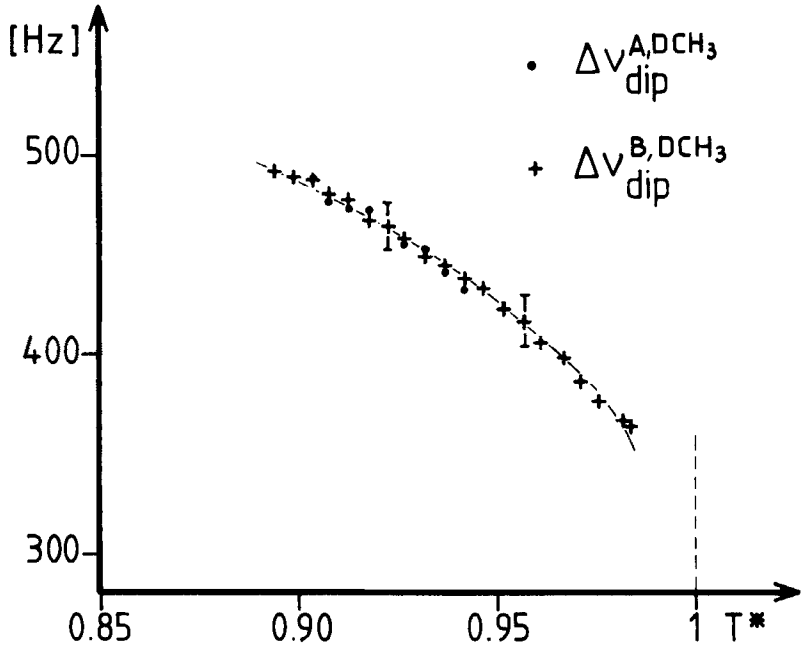

FIGURE 14 Dipolar splittings $\Delta\nu^{A,DCH_3}_{dip}$ and $\Delta\nu^{B,DCH_3}_{dip}$ measured on PAAd8 spectra (Figure 2) versus reduced temperature. For A, it cannot be measured for $T^* > 0.93$. The full curve is Eq. (14B) with $K^B_{DCH_3} = 665$ Hz and S given by Eq. (12).

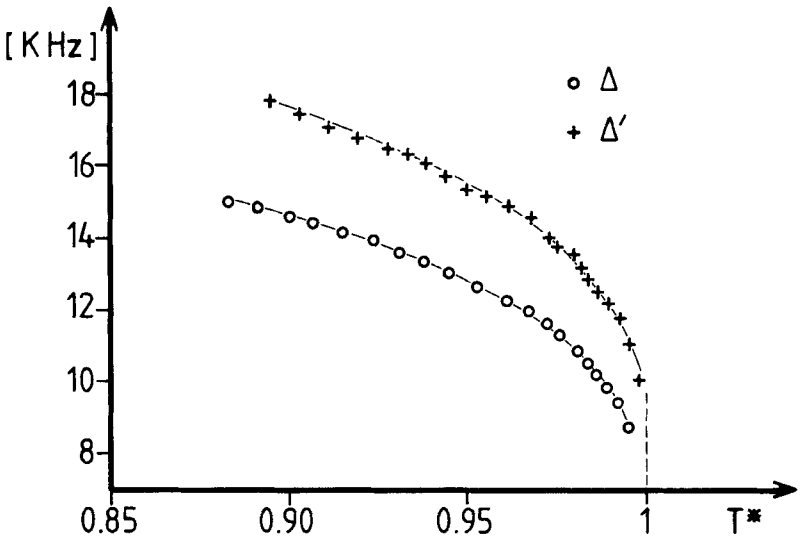

FIGURE 15 Variation of the main splittings Δ and Δ′ as defined in Figure 4a, b versus reduced temperature. The full curves are Eqs. (19) for Δ and Eq. (20) for Δ′ where S is given by Eq. (12).

where S is given by Eq. (12). The best fits are found for K_{HH} = 19.92 ± 0.02 KHz and K'_{HH} = 23.83 ± 0.06 KHz. In both cases, the temperature dependence is well reproduced.

5. SUMMARY OF THE RESULTS

5a. Influence of deuteration

The first point to be noticed is that the model can explain self-consistently all the DMR data analysed above, concerning PAAd14, PAAd8, PAAd6 and PAA with the same values of the structural and conformational parameters, provided one renormalizes properly the temperature scale to the clearing point temperature, as prescribed by theory [14]. This is particularly illustrated in Figures 10 and 11 which show that the $\Delta\nu_i/S$ are the same for all samples studied. The slight, but definite, discrepancy which exists for $\Delta\nu_2$ and $\Delta\nu_4$ is due to experimental uncertainty rather than to the model. The reason is that, although the measurement yields $\Delta\nu_2 = \Delta\nu_4$ (because the corresponding lines cannot be discriminated on PAAd14 and PAAd8 spectra) one measures accurately $\Delta\nu_2$ with PAAd14 and $\Delta\nu_4$ with PAAd8. These two splittings have no reason to be identical, being

associated with deuterons with different environment belonging to different rings. Careful examination of Figures 1 and 2 shows that $\Delta\nu_4$ is slightly larger than $\Delta\nu_2$. This is confirmed by PAAd6 data as seen in Figure 10, and by the model since calculated $\Delta\nu_4$ are in average larger than calculated $\Delta\nu_2$. The small differences in the values of the structural angles u_i found in the fits using PAAd14 and PAAd8 data mainly come from the fact that we force $\Delta\nu^A_{r_2}$ to be equal to $\Delta\nu^B_{r_1}$ in the former case, and the reverse in the latter case; and clearly these two situations are not equivalent.

At this stage of the discussion, it can thus be concluded that, at variance with what is claimed in [4], partial or complete deuteration does not induce any measurable change in molecular geometry and/or alignment of PAA in the nematic state. Using the present results, we have verified that the lineshape analysis of the PMR spectrum of PAAd6 made in reference [4], which is essential for the conclusions of [4] is not valid. (See also [11].) This will be detailed elsewhere.

5b. Nematic order parameter

The above analysis has shown that optical and NMR methods yield the same values of the nematic order parameter S. This proves that the model proposed is, *at least,* an operational model to determine S from quadrupolar and dipolar NMR splittings.

This may be very useful when using PAA as a probe in fluid anisotropic media (e.g., a nematic polymer [15–17] or mixtures of nematics) to deduce quantitative information on the degree of orientational order. More specifically, when using PAAd14 as a probe, one can use Eqs. (1A) to (6B) where the structural parameters are practically known, to analyse the quadrupolar splittings, (Figure 1) and/or the following relation:

$$\Delta\nu^{A,DD}_{dip}/\text{Hz} = 328 \cdot S \tag{16}$$

to analyse the dipolar splitting associated with anisole moiety A.

With PAAd8 (Figure 2), the procedure is identical for the quadrupolar splittings. One can also use the dipolar splittings to deduce further information, but the D—D splittings are rather imprecise, and the D—CH3 splittings depend on the actual mean conformation of the anisole moieties, which may depend on the molecular environment (cf. the Appendix).

With PAAd6 (Figure 3), the quadrupolar splittings $\Delta\nu_1$ and $\Delta\nu_2$ can be used as above. However, the dipolar splittings give more direct

information on S via the two relations

$$\Delta\nu_{dip}^{A,HD}/\text{Hz} = 2137 \cdot S \tag{17}$$

$$\Delta\nu_{dip}^{B,HD}/\text{Hz} = 2029 \cdot S \tag{18}$$

Finally, for PMR (Figure 4), one can probably use with some confidence the following two relations:

$$\Delta/\text{KHz} = 19.92\ S \tag{19}$$

$$\Delta'/\text{KHz} = 23.83\ S \tag{20}$$

for PAAd6 and PAA respectively.

5c. The structural parameters

Strictly speaking, the angles u_r and u_m are not structural angles, but rather mean angles between chemical bonds and the effective internal rotation axes $Oz_{A,B}$ (Figure 5). The $\epsilon_{A,B}$ are the inclinations of these axes on the long molecular axis Oz_o. It is observed that despite the relatively large magnetic inequivalence of the various deuterons, as revealed by the DMR spectra, the actual structures of the two anisole moieties are nearly the same, since the angles u do not differ by more than 1°, and the ϵ by 0.51°.

Using the values of ϵ_A and ϵ_B, K_{HD}^A and K_{HD}^B, and combining Eqs. (6A, B) and (7A, B), one can deduce the distances r_A and r_B between orthoprotons of the rings. The result is $r_A = 2.493$ Å and $r_B = 2.530$ Å, to be compared with $r = 2.48$ Å in benzene.

These values of angles and distances are essentially the same as those found in other works [2, 6, 7, 9] and will not be commented further here.

5d. Conformational parameters

The main result concerning the conformation of PAA in the nematic phase is the finding that T_A and T_B are the same to a very good approximation and that their values are negative. Since the $\langle\cos 2\psi'\rangle$ are essentially positive quantities, Eqs. (4A, B) and the results pictured in Figure 9 show that $|\phi_A|$ and $|\phi_B|$ are larger than 45°. In particular, at low temperature in the nematic phase where $T_A \sim T_B$

~ -0.7, these equations show that we necessarily have

$$67° < \phi_A, \phi_B < 90° \tag{21}$$

The other important result is the finding that T_{AM} (resp. T_{BM}) is proportional to T_A (resp. T_B). This proportionality reflects a constraint for the conformation and/or dynamics of the anisole moieties. The simplest constraint is to assume that, on the time scale corresponding to the internal rotations described by the current angle ψ', each anisole moiety is rigid (see also the Appendix). Rotation of the anisole moieties as a whole around the N—ϕ bonds is then described by the single angle ψ' (or ψ'_M) and implies that we have $\langle \cos 2\psi' \rangle = \langle \cos 2\psi'_M \rangle$. Combining Eqs. (4A, B), (5A, B) with (10A, B) yields

$$\cos 2\phi_{AM} = \lambda_A \cos 2\phi_A \tag{22A}$$

and a similar Equation for B.

On the other hand, ϕ_A and ϕ_{AM} are related to the dihedral angle α_{AM} between the ring and the corresponding methoxy group (cf. Figure 5). In the Appendix, we show that $\alpha_{AM} \approx 35.5°$. The only possible relation between ϕ_A and ϕ_{AM} which satisfies both condition (21) and Eq. (22) is

$$\phi_{AM} = \phi_A - \alpha_{AM} \tag{23A}$$

A similar equation holds for B.

Solving simultaneously Eqs. (22) and (23) with $\lambda_A = \lambda_B = -0.526$ yields $\phi_A \approx \phi_B \approx 69°$ and $\phi_{AM} \approx \phi_{BM} \approx 33.5°$. The dihedral angle α between the two rings can also be deduced. From Figure (5b) it is seen that

$$\alpha = \pi - \phi_A - \phi_B \tag{24}$$

From the above values of ϕ_A and ϕ_B, we obtain $\alpha = 42°$. In fact, Eq. (24) is rigorous only if the para-axes of the rings A and B are strictly parallel. Since this is probably not the case [2], this value of α may be off by a few degrees. Preliminary attempts to simulate the PMR spectrum of PAAd6 suggest that α is probably slightly smaller $\sim 36°$.

6. DISCUSSION

6a. Consequences of the model and comparison with other results

The above analysis has provided a number of results concerning the molecular properties of PAA in the nematic phase. Since these results are a direct consequence of the model, it is important to discuss if they are physically reasonable by comparison with results obtained by other methods.

The order parameter predicted by the model is the same as that deduced from optical and ^{13}C NMR measurements yielding a first support to the model. A stronger support is provided by the finding concerning the structure, conformation and internal motions. The fact that the rotations around the N—ϕ bonds are "easy" and much "easier" than around the ϕ—O bonds is consistent with quantum chemistry calculations concerning the isolated molecule [18]. These calculations indeed show that the barrier height around the N—ϕ bonds is smaller than 1 kcal/mol ($\approx k_B T_K$), whereas the barrier around the ϕ—O bonds is significantly higher. This may explain the rather rigid character of the anisole moieties (as implied by the model) on the time scale of the rotation around the N—ϕ bonds. Since the barrier around N—ϕ is low, in the nematic phase, this rotation is expected to be mainly governed by the intermolecular potentials. These potentials necessarily decrease as the molecular free volume (i.e. the temperature) increases, and the corresponding rotations become more and more uniform. Mathematically, this means that the $\langle \cos 2\psi' \rangle$ and consequently $|T_{A,B}|$ decrease with increasing temperature, as observed. Assuming that ϕ_A and ϕ_B remain constant and equal to 69°, $\langle \cos 2\psi' \rangle$ is found to vary from ~0.94 at low temperature (pure π flips correspond to $\langle \cos 2\psi' \rangle = 1$) to ~0.31 near the clearing point. The temperature dependence of $\langle \cos 2\phi' \rangle$ is pictured in Figure 9 since $\langle \cos 2\psi' \rangle$ is proportional to $|T_{A,B}|$.

It is interesting to compare the variation of $T_{A,B}$ with that of the molar volume [19], reproduced in Figure 16. It is seen that both quantities vary first slowly at low temperature, then more rapidly as the clearing point is approached, as expected from the above discussion. A more quantitative check of this particular point would be the following: if the molar volume is kept constant, e.g by applying pressure on the sample [20], then the $\langle \cos 2\psi' \rangle$ should exhibit a much weaker temperature dependence since the free volume does not change, and $k_B T$ varies very little over the whole nematic range. In other

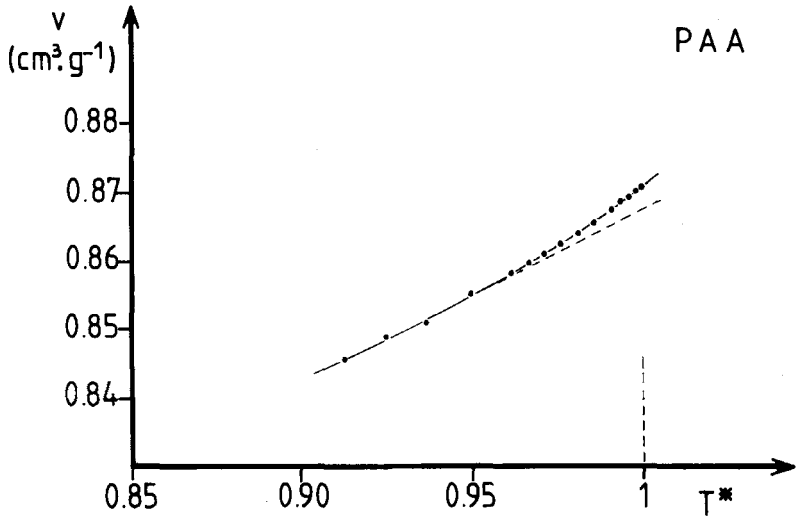

FIGURE 16 Molar volume of nematic PAA versus reduced temperature (extracted from reference [19]).

words, ratios of splittings should be nearly constant or equivalently, curves in Figures 10 and 11 should be nearly horizontal straight lines.

Another consequence of the low barrier around the N—ϕ bond is that rotation of the anisole moieties and rotation of the azoxy-group need not occur on the same time scale. Existence of easy rotation around the N—ϕ bond was first invoked in [21] to explain the apparent discrepancy between quasi-elastic neutron scattering and dielectric relaxation measurements, which show that the correlation time for rotation of the rings is much shorter than for the azoxy-group. Conversely the relative rigidity of the anisole moieties is also supported by neutron quasi-elastic scattering which shows that the correlation times for rotation of the rings, and of the methoxy groups are the same [21].

The values of the dihedral angles between molecular fragments are also of interest for the discussion. Since the density of the nematic phase is intermediate between that of the solid and gas phases, we expect that these angles, whose values are important in the determination of the molecular volume, have also intermediate values. For the dihedral angles α_{AM} and α_{BM} between rings and methoxy groups, their values are 12 and 32° in the solid phase [22] and 90° for the isolated molecule [18], to be compared with $\alpha_{AM} \approx \alpha_{BM} \approx 35.5°$ found in the present study. Concerning the dihedral angle α between the two rings, the discussion is delicate since the two rings are not

adjacent. However, we reasonably expect that its value is not smaller than in the solid phase, namely $\alpha_{solid} \approx 22.4°$ [22] to be compared with $\leqslant 42°$ found here.

Further tests for the model may be imagined. Besides the pressure experiment which would provide a general check, specific consequences of the model can be tested. For example, the changes in the degree of uniformity of the rotations of the rings around the N—ϕ bonds can be tested by a detailed analysis of the PMR line shapes of PAAd6. In Figure 4b, it is seen that the two lines of the main doublet are split into two ill-resolved lines of different intensities, mainly because of dipolar interactions between protons of different rings [11, 23]. This feature tends to smear out as temperature increases, all things being equal. In a situation where the dihedral angle α between rings is smaller than 45°, as has been found, this decrease can be qualitatively explained by assuming that the rotation of the rings becomes more and more uniform. A quantitative study of this problem will be published elsewhere and contrasted with the analysis of [4].

6b. Comments on the analysis of reference [2]

It is now interesting to understand why the results concerning S, T_A, T_B of reference [2] were found to be essentially the same as in the present work despite the fact that a wrong assignment of lines, and an incorrect assumption concerning the most probable conformation of the anisole moieties, were used. The reasons are simple: (i) we have seen that although for DMR the two anisole moieties are magnetically inequivalent, both the structure and the internal rotations are nearly the same. Consequently, it is of little importance for the model that a specific deuteron belongs to one or another fragment; this is taken into account by only slightly changing the value of the corresponding structural angle u_i, since all u_i are equal within 1.7°. (ii) in addition to be nearly equal, these angles are also very near the "magic angle" (54.74°). Thus, changing $u_m^{A,B}$ into a symmetrical value with respect to this angle and simultaneously changing the signs of T_{AM} and T_{BM} does not change the absolute values of the methyl deuteron splittings $\Delta\nu_m^{A,B}$ (Eqs. 3A, B). The results of reference [2] and of the present work correspond to these two symmetrical situations. The present data with PAAd8 concerning $\Delta\nu_{dip}^{D,CH_3}$ now excludes the possibility of reference [2] where the anisole moieties were planar. Finally, the theoretical calculations of [18] as well as the present study clearly show that the variations of $T_{A,B}$ are mainly due

to variations of $\langle \cos 2\psi' \rangle$ rather than to ϕ_A and ϕ_B. In [2], it was not possible to draw any conclusion concerning this point. We estimated there the maximum variation of ϕ_A and ϕ_B, and thus of α (cf. Eq. 24), assuming that $\langle \cos 2\psi' \rangle$ was constant.

6c. A picture of nematic phase

The model and the obtained results allow us to propose a picture for the nematic phase of PAA, concerning the various molecular motions. On a short time scale, presumably the neutron time scale ($\sim 10^{-11}$ s), the anisole moieties are rigid and rotate around the N—ϕ bonds. The C_{2v} symmetry of these rotations probably reflects the fact that they are governed by the interaction between phenyl rings of neighbouring molecules, as suggested by the structure in the solid phase [22]. On a longer time scale, the phenyl rings also perform individual π flips. On the same or even larger time scale, collective motions should be invoked. As suggested by X-ray diffraction [24], the basic entity to be considered is an ensemble of several neighbouring, parallel molecules which define a "cage" in which each molecule is able to reorient. The axis of this cage, which defines the long molecular axis, can be identified with the local nematic director of the continuum theories. Rotation around the long axis probably corresponds to reorientation of the molecules as a whole in their respective cages. Although the local structure has probably low symmetry, since the medium is fluid and uniaxial, an effective cylindrical symmetry is produced by exchange between neighbouring molecules on the time scale of lateral self-diffusion ($\sim 10^{-10}$ s) [21]. Finally, on a longer time scale ($\sim 10^{-8}$ s) the local director fluctuates about the main director mainly due to hydrodynamic modes. All these motions are fast on the DMR time scale ($\sim 10^{-6}$ s) [25].

This model where a nematic is composed with only one kind of molecule (the most probable conformation) is consistent with those used to analyse X-ray diffraction [24] and light scattering [25,26] data of nematics. It is different from other models used in connection with NMR [27,28] where a nematic is pictured as a mixture of a large number of different conformations, generally those of the isolated molecules, which exchange between themselves via the internal rotations. These kinds of models are a priori more general since separation between external and internal motions is not made, but the choice of the conformations to be considered is somewhat arbitrary. In the present model, the single conformation is not assumed a priori, but is deduced from the data.

7. CONCLUSION

In conclusion, the present study has confirmed that the simple model presented in [2] can describe self-consistently a large number of NMR data concerning the PAA molecule in the nematic phase. The deduced information concerning the structure, conformation and order is physically reasonable and in agreement with results obtained by other methods. This model provides a method to analyse similar data when PAA is used as a probe in other fluid nematic media [17]. A number of constant coefficients have been determined and useful relations between dipolar splittings and order parameter have been produced. The central feature of the model is the existence of easy rotation of the anisole moieties around the N—ϕ bonds, which is supported by both theoretical calculations and independent experiments. The main consequence of this is that the degree of uniformity of these rotations is mainly governed by the intermolecular potentials, i.e. the molecular free volume. No measurable influence of deuteration on the molecular structure and/or alignment need to be invoked to explain all the data considered.

Acknowledgment

We are indebted to Drs. J. Berges and H. Perrin for providing the results of their theoretical calculations on isolated PAA prior to publication. Thanks to them and also to Prof. J. A. Janik for fruitful discussions. This work was partially supported by JNICT, Portugal, under contract no. 424.82.68 (AFM and JBF), by the French Ministère des Relations Extérieures, under the Franco-Portuguese Scientific Cooperation Program (JBF and FV) and by NATO Research Grant no. 475.83 (AFM and FV).

APPENDIX

The fine structure of doublet $\Delta\nu_5$, associated with deuterons D_2 and D_6 of anisole moiety B (Figure 2) is easily explained. Dipolar interaction with the three equivalent (due to fast rotation [29]) methyl protons, splits each component into 4 equidistant lines with relative intensities 1:3:3:1, separated by $\Delta\nu_{dip}^{B,DCH_3}$. Dipolar interaction with deuterons D_3 and D_5 (non equivalent to D_2 and D_6) further splits each of these lines into three (nearly) equidistant lines with (nearly) relative intensities 1:1:1 separated by $\Delta\nu_{dip}^{B,DD}$. Both effects superpose. In a situation where $\Delta\nu_{dip}^{B,DCH_3} \approx 2\Delta\nu_{dip}^{B,DD}$, each component is ultimately split into 9 lines of relative intensities 1:1:4:3:6:3:4:1:1, as

observed in Figure 2, where it is easy to point the corresponding two splittings. (idem for moiety A).

In order to calculate $\Delta\nu_{dip}^{B,DCH_3}$, we have to perform a three step calculation. (i) first we have to calculate the dipolar splitting of deuterons D_2 and D_6 due to a proton M moving (uniformly) on a circle of center P, as sketched in Figure 17, (ii) we must average for rotation of the anisole moiety as a whole around the N—ϕ bond and (iii) we must further average this splitting for exchange between D_2 and D_6 which are magnetically equivalent due to π flips of the ring. For the first step, we have, for deuteron D_2 (and similarly for D_6)

$$\delta_{D_2} = -\frac{h\gamma_H\gamma_D}{2\pi^2}\frac{\overline{P_2(\cos\tau_2)}}{|D_2M|^3} \tag{A1}$$

where τ_2 is the angle between D_2M and the long axis Oz_0 and $h\gamma_H\gamma_D/2\pi^2 = 36.884$ KHz.Å^3 The bar stands for average over rotation on the circle of radius PM. Choosing reference frames and defining symbols as indicated in Figure 17, with x_B in the plane of the ring and z_B along the para-axis, Px' in the plane (z_B, OP) and z' along

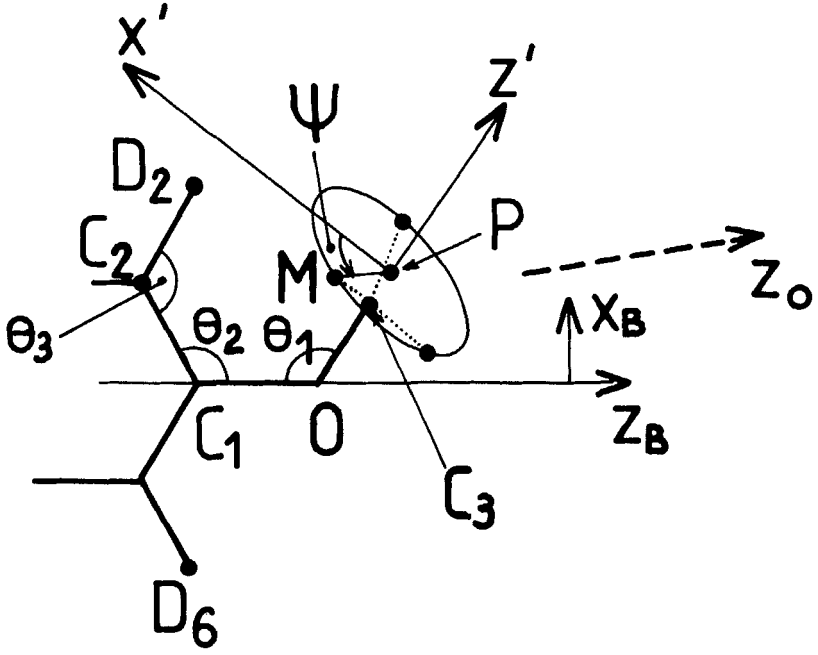

FIGURE 17 Sketch of anisole moiety B defining the various symbols which are useful in the calculation of δ_{D_2} in Eq. (A1).

OP, the components of any vector are easily calculated. In the x_B, y_B, z_B frame, we have

(i) for D_2P and D_6P

$$x_{D_2P} = d_1 \sin\theta_1 \cos\alpha_{BM} - d_3 \sin\theta_2 + d_4 \sin(\theta_2 + \theta_3) \tag{A2}$$

$$x_{D_6P} = d_1 \sin\theta_1 \cos\alpha_{BM} + d_3 \sin\theta_2 - d_4 \sin(\theta_2 + \theta_3) \tag{A3}$$

$$y_{D_2P} = y_{D_6P} = d_1 \sin\theta_1 \sin\alpha_{BM} \tag{A4}$$

$$z_{D_2P} = z_{D_6P} = -d_1 \cos\theta_1 + d_2 - d_3 \cos\theta_2 + d_4 \cos(\theta_2 + \theta_3) \tag{A5}$$

(ii) for PM

$$x_{PM} = \rho \cos u_m^B \cos\alpha_{BM} \cos\psi - \rho \sin\alpha_{BM} \sin\psi \tag{A6}$$

$$y_{PM} = \rho \cos u_m^B \sin\alpha_{BM} \cos\psi + \rho \cos\alpha_{BM} \sin\psi \tag{A7}$$

$$z_{PM} = -\rho \sin u_m^B \cos\psi \tag{A8}$$

where α_{BM} is the dihedral angle between the ring and methoxy group of B. The values of the various distances and angles are:

$d_1 = OC_3 + C_3P = 1.431 + 0.363 = 1.794$ Å,
$d_2 = C_1O = 1.352$ Å

$d_3 = C_1C_2 = 1.394$ Å, $d_4 = C_2D_2 = C_6D_6 = 1.084$ Å (all these values are deduced from [18], $\rho = PM = 1.032$ Å (from [29]), $\theta_1 = \pi - u_m^B = 122.40°$, $\theta_2 = 120°$, $\theta_3 = (\pi/3) + u_{r_2}^B = 116.22°$, $\epsilon_B = 15.61°$ (deduced from the present study).

For the second step of the calculation, introducing the most probable frame x_B^m, y_B^m, z_B^m with $z_B^m = z_B$ such as $(x_B, x_B^m) = \psi_B'$, we have, for vector D_2M (and similarly for D_6M)

$$x_{D_2M}^m = x_{D_2M} \cos\psi_B' + y_{D_2M} \sin\psi_B' \tag{A9}$$

$$y_{D_2M}^m = x_{D_2M} \sin\psi_B' - y_{D_2M} \cos\psi_B' \tag{A10}$$

$$z_{D_2M}^m = z_{D_2M} \tag{A11}$$

In this fixed frame, the polar and azimuthal angles of the long axis Oz_0 are just ϵ_B, ϕ_B.

Averaging for the rotation described by ψ'_B is performed using a function of C_{2v} symmetry (required by the model) of the form

$$p(\psi'_B) = \frac{1}{Z} \exp(\gamma' \cos 2\psi'_B) \tag{A12}$$

where Z is a normalisation contant and where γ', or equivalently the parameter $\langle \cos 2\psi'_B \rangle$ defined as

$$\langle \cos 2\psi'_B \rangle = \frac{1}{Z} \int_{(2\pi)} \cos 2\psi'_B \, p(\psi'_B) \, d\psi'_B \tag{A13}$$

describe the degree of uniformity of this rotation.

For the third step, we must average the splittings obtained with D_2 and D_6. Thus, the theoretical expression of the splitting δ^{B,DCH_3} is ultimately a function of the parameters α_{BM},ϕ_B and $\langle \cos 2\psi'_B \rangle$, namely:

$$\delta^{B,DCH_3}(\alpha_{BM}, \phi_B, \langle \cos 2\psi'_B \rangle) = \frac{1}{2} \int_{(2\pi)} (\delta_{D_2} + \delta_{D_6}) \, p(\psi'_B) \, d\psi'_B \tag{A14}$$

This expression was evaluated by numerical integration over ψ and ψ'_B for various values of the parameters. It turns out that its numerical value is practically independent of both ϕ_B and $\langle \cos 2\psi'_B \rangle$ but is a strong function of α_{BM}. This is illustrated in Figure 18 which shows the values of δ^{B,DCH_3} versus $\langle \cos 2\psi'_B \rangle$ for a fixed value of ϕ_B and various values of α_{BM}. The independence with $\langle \cos 2\psi'_B \rangle$ is completely consistent with experiment which shows that, contrary to the quadrupolar splittings, the dipolar splittings $\Delta\nu_{dip}^{D,CH_3}$ depend on temperature via S only (Eq. 14), and implies that in the nematic phase α_{BM} (and α_{AM}) is practically constant. The value of this angle can be estimated from Figure 18. Since $S = 1$ in this calculation, putting $\delta^{B,DCH_3} = K^B_{DCH_3} \approx 665$ Hz (cf. Eq. 14B), we find $\alpha_{BM} \approx 35.5° \approx \alpha_{AM}$.

Besides the fact that the most probable angle α_{BM} is temperature independent, the model also implies that on the time scale of the rotation described by ψ'_B, the anisole moieties are rigid. Indeed, a more complicated calculation permitting independent rotations of the

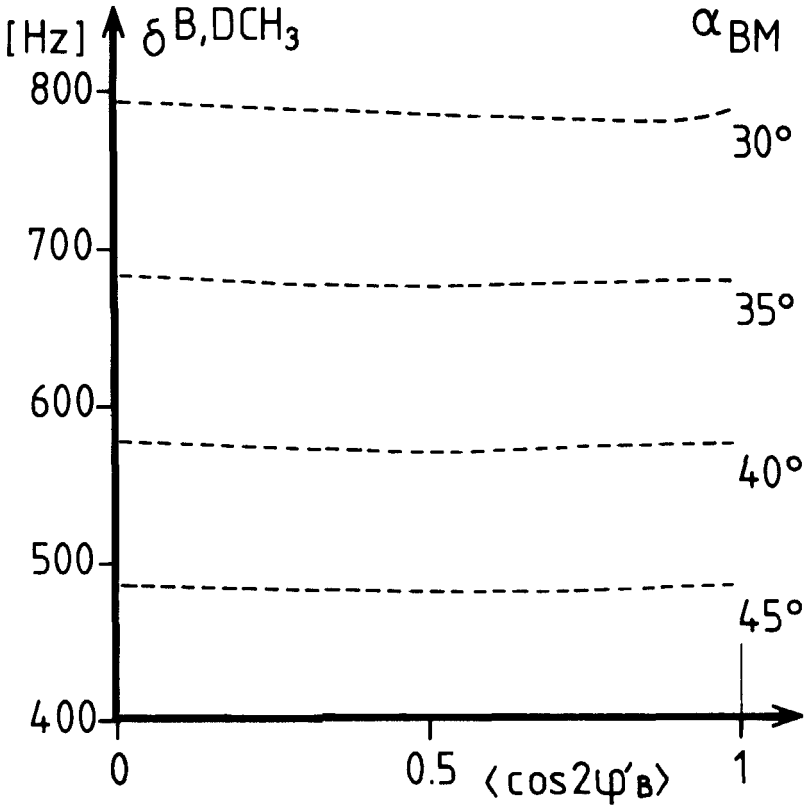

FIGURE 18 Theoretical variation of δ^{B,DCH_3} given by Eq. (A14) versus $\langle \cos 2\ \psi'_B \rangle$ for various values of α_{BM}, and $\phi_B = 69°$. For other values of ϕ_B, the curves are the same within less than 1%.

ring and of the methoxy group around Oz_B predicts an important dependence of δ^{B,DCH_3} with $\langle \cos 2\psi'_B \rangle$, which is not observed.

In conclusion, analysis of the dipolar splittings between ring deuterons and methyl protons provides a test for the model and permits the determination of the dihedral angle between rings and methoxy groups.

References

1. A. J. Dianoux and F. Volino, *J. Physique*, **41**, 1147 (1980).
2. F. Volino, A. F. Martins, and A. J. Dianoux, *Mol. Cryst. Liq. Cryst.*, **66**, 37 (1981).
3. F. Volino, A. J. Dianoux, J. Berges, and H. Perrin, *Mol. Cryst. Liq. Cryst.*, **90**,

281 (1983); some errors were detected in this paper after publication; they affect some (important) details, but not the general qualitative results.
4. K. Hayamizu and O. Yamamoto, *J. Magn. Reson.*, **41**, 94 (1980).
5. J. W. Emsley and D. L. Turner, *Chem. Phys. Lett.*, **82**, 447 (1981).
6. P. Diehl and A. S. Tracey, *Mol. Phys.*, **30**, 1917 (1975).
7. J. W. Emsley, S. K. Khoo, and G. R. Luckhurst, *Mol. Phys.*, **37**, 959 (1979).
8. R. Y. Dong, J. Lewis, E. Tomchuk, Chas. G. Wade, and E. Bock, *J. Chem. Phys.*, **74**, 633 (1981).
9. P. Diehl, H. Huber, A. C. Kunwar, and M. Reinhold, *Org. Mag. Res.*, **9**, 374 (1977).
10. J. W. Emsley, J. C. Lindon, and J. M. Street, J.C.S. Perkin II, 805 (1976).
11. St. Limmer, H. Schmiedel, B. Hillner, A. Lösche, and S. Grande, *J. Physique*, **41**, 869 (1980).
12. P. J. Bos and J. W. Doane, *Phys. Rev. Lett.*, **40**, 1030 (1978).
13. E. G. Hanson and Y. R. Shen, *Mol. Cryst. Liq. Cryst.*, **36**, 193 (1976).
14. See e.g. P. G. de Gennes "*The Physics of Liquid Crystals*" (Oxford University Press, London, 1974).
15. R. B. Blumstein, A. Blumstein, E. M. Stickles, M. D. Poliks, A. M. Giroud, and F. Volino, Polymer Preprints, **24**, N°2, 275, August 1983.
16. F. Volino and R. B. Blumstein, *Proceedings of the 4th European Winter Conference on Liquid Crystals of Low-Dimensional Order and Their Applications,* Bovec, Yugoslavia, 26–30 March 1984, *Mol. Cryst. Liq. Cryst.* (in print)
17. F. Volino, A. M. Giroud, A. J. Dianoux, R. B. Blumstein, and A. Blumstein, Paper presented at the 10th International Liquid Crystal Conference, York, UK, 15–21 July 1984, *Mol. Cryst. Liq. Cryst.* (in print)
18. J. Berges and H. Perrin, a) *J. Chimie Physique,* **78**, 573 (1981); b) *Proceedings of the 4th European Winter Conference on Liquid Crystals of Low-Dimensional Order and Their Applications,* Bovec, Yugoslavia, 26–30 March 1984, *Mol. Cryst. Liq. Cryst.* (in print) c) *J. Physique*, 45 Dec 1984.
19. W. Maier and A. Saupe, *Z. Naturforsch.*, **15a**, 287 (1960).
20. J. W. Emsley, G. R. Luckhurst, and B. A. Timimi, *Mol. Phys.*, **46**, 659 (1982).
21. a) J. A. Janik, J. M. Janik, and K. Otnes, in "*Liquid Crystals,*" Proceedings of the Bangalore Conference, ed. S. Chandrasekhar, Heyden Publisher (1979), p. 391; b) J. A. Janik, *Advances in Liquid Crystals,* **5**, 315 (1982).
22. W. R. Krigbaum, Y. Chatani, and P. G. Barber, *Acta Cryst.*, **B26**, 97 (1970).
23. A. F. Martins, *Portugal Phys.*, **8**, 1 (1972).
24. A. J. Leadbetter and E. K. Norris, *Mol. Phys.*, **38**, 669 (1979).
25. M. Warner, *Mol. Phys.*, **52**, 677 (1984).
26. T. E. Faber, *Proc. Roy. Soc. (London),* **A353**, 247 (1977).
27. E. T. Samulski and R. Y. Dong, *J. Chem. Phys.*, **77**, 5090 (1982).
28. J. W. Emsley, G. R. Luckhurst, and C. P. Stockley, *Proc. R. Soc. (London),* **A381**, 117 (1982).
29. H. Hervet, A. J. Dianoux, R. E. Lechner, and F. Volino, *J. Physique,* **37**, 587 (1976).